Engineering Optical and Electronic Properties of WS_2 by Varying the Number of Layers

Hyun-Cheol Kim,[†,⊥] Hakseong Kim,[†,⊥] Jae-Ung Lee,[§] Han-Byeol Lee,[†] Doo-Hua Choi,[†] Jun-Ho Lee,[†] Wi Hyoung Lee,[‡] Sung Ho Jhang,[†] Bae Ho Park,[†] Hyeonsik Cheong,[§] Sang-Wook Lee,[†] and Hyun-Jong Chung*[,†]

[†]Division of Quantum Phases and Devices, Department of Physics, Konkuk University, Seoul 143-701, Korea, [‡]Department of Organic and Nano System Engineering, Konkuk University, Seoul, 143-701, Korea, and [§]Department of Physics, Sogang University, Seoul 121-742, Korea. [⊥]These authors contributed equally.

ABSTRACT The optical constants, bandgaps, and band alignments of mono-, bi-, and trilayer WS_2 were experimentally measured, and an extraordinarily high dependency on the number of layers was revealed. The refractive indices and extinction coefficients were extracted from the optical-contrast oscillation for various thicknesses of SiO_2 on a Si substrate. The bandgaps of the few-layer WS_2 were both optically and electrically measured, indicating high exciton-binding energies. The Schottky-barrier heights (SBHs) with Au/Cr contact were also extracted, depending on the number of layers (1−28). From an engineering viewpoint, the bandgap can be modulated from 3.49 to 2.71 eV with additional layers. The SBH can also be reduced from 0.37 eV for a monolayer to 0.17 eV for 28 layers. The technique of engineering materials' properties by modulating the number of layers opens pathways uniquely adaptable to transition-metal dichalcogenides.

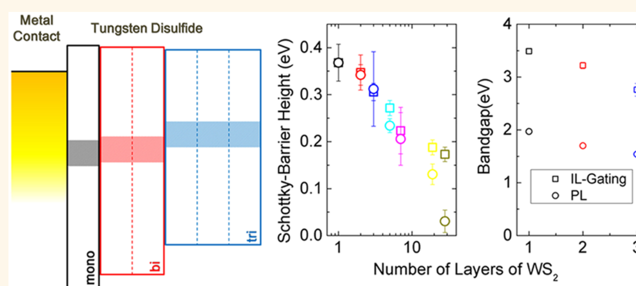

KEYWORDS: tungsten disulfide · transition-metal dichalcogenide · bandgap · band-alignment · Schottky barrier

Recently, two-dimensional (2D) semiconductors have drawn considerable attention as strong candidates for next-generation electronic and optoelectronic devices such as transistors, barristors, and photosensors owing to their exotic properties.[1−7] Transition metal dichalcogenides (TMDs) provide fine bandgap tenability: the various TMDs not only allow a wide bandgap range, but also enable the bandgap to be tuned according to the TMD thickness.[8,9] Highly stable excitons also show promise for improving optoelectronic devices.[10] In addition, subnanometer thickness and flexibility of the TMDs would open new applications.[11−15] Among the TMDs, WS_2 is uniquely interesting for barristor devices because its conduction band seems aligned to the Dirac point of graphene, and therefore, the current between graphene and WS_2 can easily be turned on and off by modulating the graphene's work function.[1,4]

However, the fundamental properties of the material for electronic and optoelectronic application have not yet been fully addressed. For example, owing to the large exciton-binding energy, the bandgap of monolayer WS_2 has been highly controversial—the experimental ones span from 2.14 eV (IL-gating method) to 2.9 eV (absorption/reflectivity measurement); the theoretical ones do from 1.55 eV (*ab initio*) to 3.11 eV (self-consistent GW_0, scGW_0).[8,10,16,17] Recently, two-photon excitation spectroscopy along with GW plus Bethe-Salpeter equation (GW-BSE) theory measured 2.7 eV.[18−20] However, optical absorption/reflectivity measurement and self-consistent GW_0 calculation reports greater bandgap—2.9 and 3.11 eV, respectively.[10,17] In contrast, IL-gating method reports smaller ones—2.14, 1.82, and 1.4 eV for monolayer, bilayer, and bulk WS_2, respectively, and scanning tunneling spectroscopy (STS) has not been applied for WS_2 but for MoS_2 and $MoSe_2$.[21,22] In addition, band alignment, another materials property critically affecting the device performance, has not yet been investigated.

* Address correspondence to hjchung@konkuk.ac.kr.

Received for review January 12, 2015 and accepted July 4, 2015.

Published online July 04, 2015
10.1021/acsnano.5b01727

© 2015 American Chemical Society

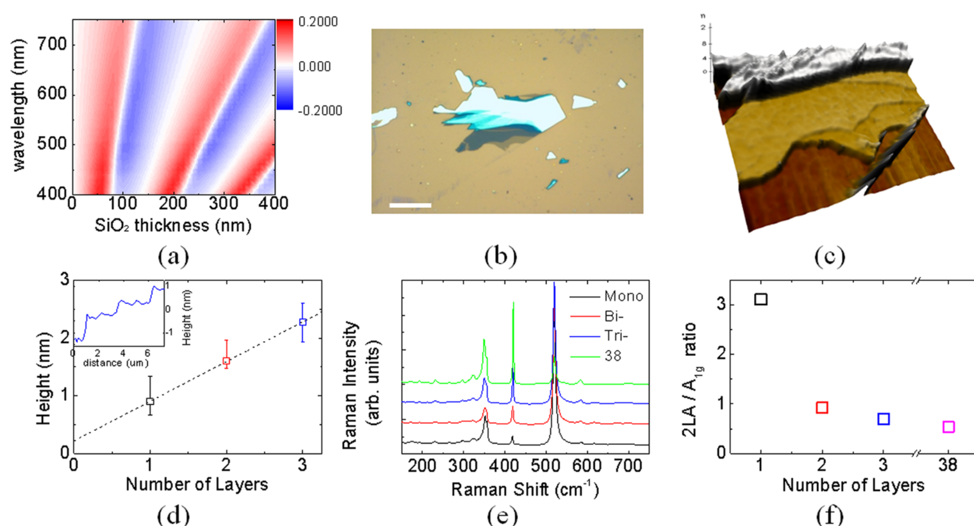

Figure 1. Location of few-layer WS_2 and identification of thickness using AFM and Raman spectroscopy. (a) Optical-contrast map of monolayer WS_2 depending on thickness of SiO_2 and wavelength of light, with *n* as 3–3.15 and *k* as 1.04–0.44, depending on the wavelength,[23] and thickness of the monolayer as 0.65 nm. (b) Optical-microscopy image of WS_2 flake on 90 nm SiO_2/Si, where scale bar represents 10 μm. (c) 3D AFM image of same flake, where mono-, bi-, and trilayer WS_2 are clearly shown. (d) Linearly fitted thickness of WS_2, where thickness of single layer is 0.69 nm, and first layer has extra thickness of 0.22 nm. (Inset) Height profile measured using AFM. (e) Raman spectroscopy using 514.4 nm-wavelength laser. (f) 2LA(M)/$A_{1g}(\Gamma)$ intensity ratio, where intensity ratio decreases with thickness and is saturated around 0.5 for bulk WS_2. Additional peaks are observed because of the resonance effect.

The refractive index (*n*) and extinction coefficient (*k*) have been measured for bulk WS_2 but not for few-layer WS_2.[23] In the present study, essential materials properties for the electronic and optoelectronic applications of mono-, bi-, and trilayer WS_2 were measured. The optical constants (*n* and *k*) were precisely obtained from contrast oscillation, depending on thickness of the SiO_2 on Si substrates. The bandgap of the few-layer WS_2 was electrically measured and, as a result, a large exciton-binding energy was experimentally estimated. In particular, its unusually high dependency on the thickness was discovered: a single layer yields extraordinarily different material properties. In addition, Schottky-barrier reduction with the thickness was observed, leading to band alignment for the mono-, bi-, and trilayer WS_2.[24]

RESULTS AND DISCUSSION

Location of Few-Layer WS_2. The low optical contrast of 2D materials should be maximized before the materials are located by optical microscopy.[25−27] Figure 1a shows the calculation of the contrast of the WS_2 monolayer. Similarly to other 2D materials, the contrast exhibits an oscillation depending on the thickness of the SiO_2 on the Si. While only a positive contrast (flakes darker than SiO_2) is observed for the monolayer graphene,[25] a negative contrast (flakes brighter than SiO_2) is expected for ~120 nm SiO_2/Si, similarly to the case of h-BN.[26] The maximum contrast is more than double that of monolayer graphene for 600 nm-wavelength light on 300 nm SiO_2, whereas the minimum-negative contrast is almost 0.1 for 750 nm light. Therefore, 90 nm SiO_2/Si was selected to locate the few-layer WS_2 flakes, as shown in Figure 1b, and then, the flakes' thickness was confirmed by atomic force microscopy (AFM) and Raman spectroscopy, as shown in Figure 1b−f. Figure 1c shows a three-dimensional (3D) mapping measured by AFM. Here, the line profile confirms that the thickness of the first layer on the SiO_2 measures 0.9 nm, and that of the second and later layers measures 0.65 nm. The van der Waals force between the WS_2 layers could be stronger than the force between the WS_2 and SiO_2; for the former, the layers' surfaces are atomically flat, and the periodicities are perfectly matched with each other. This discrepancy could also originate from impurities (N_2, O_2, Ar, or H_2O) between the SiO_2 and WS_2.[28] Figure 1e shows Raman spectra, which are widely used to determine the number of layers of 2D materials.[29−31] While the A_{1g} peak at 420 cm^{-1} has a very small dependence on the number of layers, the second-order Raman mode of two longitudinal acoustic phonons at the M point (2LA(M) at 350 cm^{-1}) is the most prominent feature.[30,32] The intensity ratio of the 2LA(M) peak to the A_{1g} peak exhibits a clear dependence on the number of layers.[32] The change in this ratio is consistent with the AFM and previous reports.[30]

Refractive Index and Extinction Coefficient. The optical constants (*n* and *k*) were precisely obtained as shown in Figure 2, using the inverse of the process for calculating the contrast oscillation shown in Figure 1a. Four flakes of the few-layer WS_2 were observed on the 90 nm SiO_2, whose thicknesses were confirmed as described in Figure 1. Then, the flakes were transferred to various thicknesses of SiO_2/Si (Supporting Information Table S1). The contrast oscillation with respect to

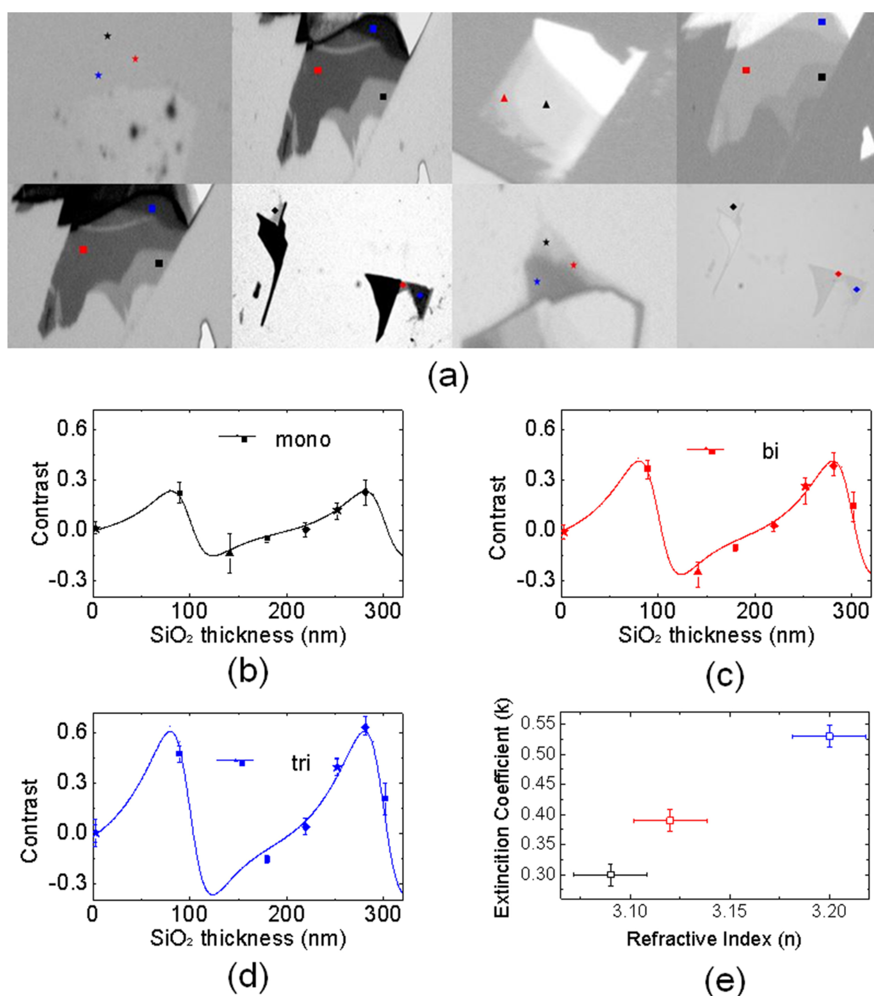

Figure 2. Extraction of *n* and *k* for few-layer WS_2 from their contrast oscillation on SiO_2/Si substrates of various thicknesses. (a) Optical images of few-layer WS_2 on 2.9, 90, 141, 180, 220, 252, 281, and 302 nm SiO_2/Si substrates (clockwise from upper-left image) using 620 nm-wavelength bandpass filter, where black, red, and blue dots correspond to mono-, bi-, and trilayer WS_2, respectively, and star, diamond, square, and triangle indicate the four flakes transferred to the various substrates. (b−d) Measured optical contrasts for mono-, bi-, and trilayer WS_2, respectively, on various substrates, along with best-fitted oscillations (solid lines),[25] where color and shape symbols have same meaning as in optical images in (a). (e) Extracted *n* and *k* of few-layer WS_2.

the SiO_2 thickness is shown in Figure 2b−d, where the oscillation is fitted to the result with *n* as 3.09, 3.12, and 3.20 and *k* as 0.30, 0.39, and 0.53 for the mono-, bi-, and trilayer WS_2, respectively (Figure 2e). The increase in *n* with the thickness reflects the decrease in the bandgap (S2).

Bandgap and Exciton-Binding Energy. We now consider the bandgap of the mono-, bi-, and trilayer WS_2. While the photoluminescence (PL) is widely used to measure the bandgap of 3D semiconductors,[33] its application to 2D semiconductors requires meticulous care, as *ab initio* calculations predict stable excitons with a binding energy as high as 0.5−1 eV for few-layer TMDs.[10,18,19,34,35] Figure 3a shows the measurement of the optical bandgap using the PL spectra of the few-layer WS_2. Two peaks are observed in the PL spectra: at 630 nm (2.0 eV) and around 720−810 nm (1.5−1.7 eV). The peak at 630 nm corresponds to the energy of the A exciton in WS_2,[36] whose peak positions do not clearly depend on the number of layers. On the other hand, the other peaks in the range of 1.5−1.7 eV arise from the indirect bandgap of the few-layer WS_2, whose peak positions clearly depend on the number of layers, owing to the change in the electronic band structure as a function of the thickness.[37] Figure 3b shows one of the WS_2 devices fabricated to electrically measure the bandgap and band alignment. Ionic liquid (IL) was used as the gate dielectric because its capacitance is high enough to directly extract the bandgap from the applied gate voltage (Supporting Information Figure S2).[38] The transfer characteristics of the representative devices are shown in Figure 3c. The mono-, bi-, and trilayer WS_2 have threshold voltages of −1.42, −1.37, and −1.51 V for the hole side and 2.07, 1.87, and 1.34 V for the electron side, respectively, at V_D = 100 mV. The differences between the two threshold voltages correspond to the bandgaps of 3.49, 3.22, and 2.76 eV for monolayer, bilayer, and trilayer WS_2 devices, respectively.

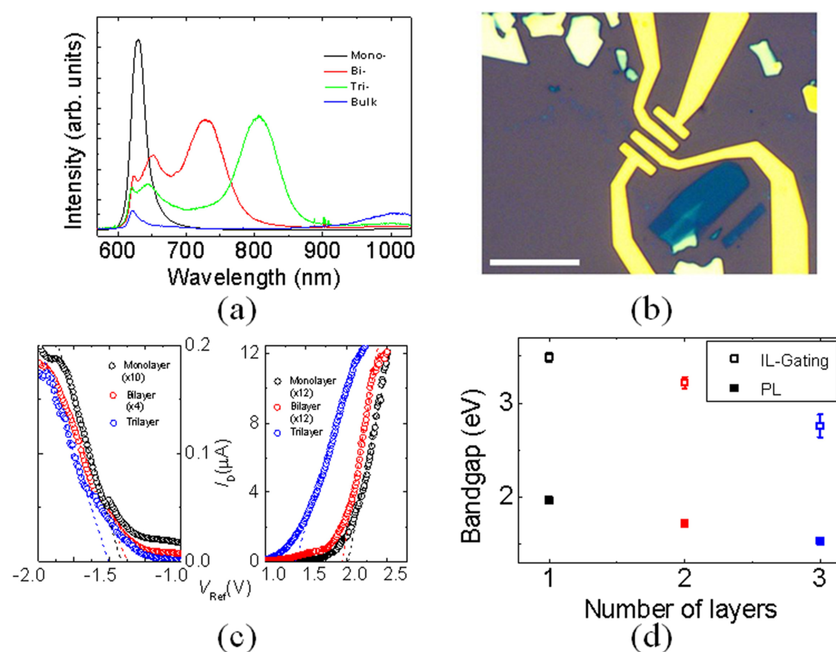

Figure 3. Measurement of bandgap of mono-, bi-, and trilayer WS_2. (a) PL measurement of few-layer and bulk WS_2. (b) Optical microscopy image of one of the fabricated devices, used to measure electrical properties. Scale bar represents 10 μm. (c) Drain-current modulation with ionic-liquid (IL) gating to electrically measure bandgap. (d) Electrical and optical bandgaps of mono-, bi-, and trilayer WS_2.

As mentioned earlier, the bandgap of monolayer WS_2 is still controversial. Calculated bandgaps span 2.41–3.11 eV; experimentally measured ones span 2.7–2.91 eV, excluding initial studies.[10,16,17,19,39] While our measurement of monolayer WS_2 is much greater than the measurement by two-photon excitation spectroscopy along with GW-BSE theory, it is only 10% greater than self-consistent GW_0 calculation for unstrained WS_2 monolayer. Still, more study including IL-gating method and STS measurement should be conducted to discover the bandgap of the few-layer WS_2.[21,22]

The exciton-binding energy originates from the Coulomb interaction between the electrons and the holes of the excitons and therefore was measured using the difference between the electrically measured bandgap (open squares shown in Figure 3d) and optically measured exciton energy (solid squares shown in Figure 3d). Therefore, the upper bound of the exciton-binding energies for mono-, bi- and trilayer WS_2 is estimated to be as large as 1.52, 1.45, and 1.20 eV, respectively. These energies not only are far greater than that of 3D semiconductors (<tens of meV), but are even greater than that of semiconducting carbon nanotubes (CNTs) (~0.4 eV). This originates from 2D nature of enhanced *e*–*h* coupling from the strong confinement in the few-layer WS_2. Therefore, the binding energy decrease as the number of layers increases.

SBH and Band Alignment. Next, the SBH (Φ_B) was measured between the WS_2 (monolayer 1 to 28 layers) and metal (Au/Cr) both the variable- (Figure 4a–d) and fixed-temperature methods (Figure 4e).[35] For the former, the *I*–*V* characteristics of layered WS_2 FETs are measured at various temperatures (260–380 K). To derive the saturation current (I_0), we use the approximation in eq 1 for $qV \gg k_BT$.[40]

$$\begin{aligned} \frac{I}{I_0} &= e^{qV/kT} - 1 \approx e^{qV/kT} (\because qV \gg kT) \\ \ln(I) &= \frac{q}{kT}V + \ln(I_0) \end{aligned} \tag{1}$$

An intercept, $\ln(I_0)$, can be extracted from the plot of $\ln(I)$ *versus* V_D, as shown in Figure 4a–c. The SBH is determined from the slope of $\ln(I_0/T^2)$ *versus* $1/T$; A^* is from the intercept, as described in eq 2.

$$\begin{aligned} I_0 &= AA^*T^2e^{-\Phi_B/kT} \\ \ln(I_0/T^2) &= \ln AA^* - \frac{\Phi_B}{k}\frac{1}{T} \end{aligned} \tag{2}$$

The monolayer exhibits the highest slope of 0.36 eV between the WS_2 and Cr/Au contact. As the number of layers increases, the SBH decreases—0.34, 0.30, 0.27, 0.22, 0.18, and 0.17 eV for 2-, 3-, 5-, 7-, 19-, and 28-layer WS_2, respectively—owing to the increase in the electron affinities of the WS_2 with the thickness.[9] A^* also decreases with the number of layers as shown in Supporting Information Figure S3.

For the latter, the SBHs were extracted from the diode equation, as shown in eq 3.

$$\begin{aligned} I_D &= AA^*e^{-q\Phi_B/kT}(e^{qV_D/kT} - 1) \\ &\text{or} \\ \Phi_B &= \frac{kT}{q}\ln\left(\frac{AA^*(e^{qV_D/kT} - 1)}{I_D}\right) \end{aligned} \tag{3}$$

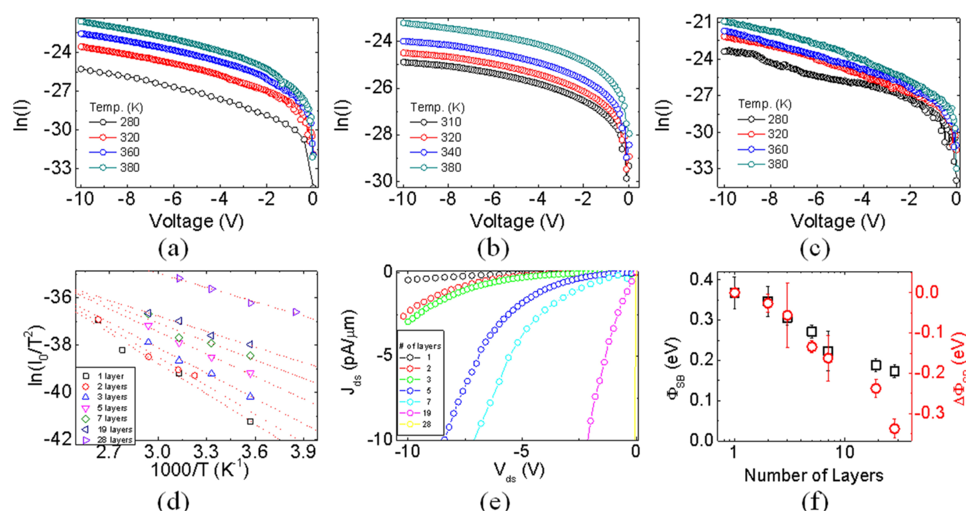

Figure 4. Measurement of SBHs between Cr/Au electrode and WS_2 for 1- to 28-layer WS_2 at varying temperatures (a−d) and room temperature (e). Logarithm plot of drain current as a function of drain voltage in (a) monolayer, (b) bilayer, and (c) trilayer WS_2 field-effect transistors. (d) Saturation current of WS_2 at various temperatures (260−380 K), where slopes decrease with thickness, as does SBH, as shown in (f). (e) Schottky current of 1- to 28-layer WS_2 at room temperature. (f) Two methods—fixed and variable temperature—result in barrier heights within errors, except for 28-layer WS_2, where Φ_B is distinguishably lower for fixed-temperature method. Although the modeling for the junction with a low barrier, nearly an Ohmic junction, has yet to be investigated clearly, the large discrepancy in Φ_B of the 10-layer or thicker WS_2 suggests the transition from a Schottky to Ohmic junction.

The difference in the SBH ($\Delta\Phi_B$) between mono- and few-layer WS_2 can be precisely extracted by dividing the diode current of the few-layer WS_2 by that of the monolayer as shown in eq 4, where we compare the drain currents of the mono- and few-layer WS_2 at the same bias voltage using the previously extracted A^*.

$$\begin{aligned}\Phi_{f.B} - \Phi_{m.B} &= \Delta\Phi_B \\ &= \frac{kT}{q}\ln\left(\frac{I_{m.D}}{I_{f.D}}\frac{A_{f.D}}{A_{m.D}}\frac{A^*{}_{f.D}}{A^*{}_{m.D}}\frac{e^{qV_{f.D}/kT}-1}{e^{qV_{f.D}/kT}-1}\right) \\ &= \frac{kT}{q}\ln\left(\frac{I_{m.D}}{I_{f.D}}\frac{A_{f.D}}{A_{m.D}}\frac{A^*{}_{f.D}}{A^*{}_{m.D}}\right)\end{aligned} \tag{4}$$

Thus, the $\Delta\Phi_B$ values of 2- to 28-layer WS_2 are extracted from Figure 4a as −0.026, −0.056, −0.134, −0.162, −0.237, and −0.337 eV (Figure 4f). The measurement of Φ_B according to the thickness yields two important discoveries. First, the band alignments—the energy difference of the conduction band or valence band among the few-layer WS_2—were estimated by comparing Φ_B values. Second, the Schottky barrier was reduced to ~0.1 eV, suggesting the possibility of an Ohmic junction for thick WS_2.

CONCLUSION

In conclusion, bandgaps of few-layer WS_2 greater than those from the initial reports[8,16,36] were electrically measured: 3.49 eV for the monolayer WS_2, 3.22 eV for the bilayer WS_2, and 2.76 eV for the trilayer WS_2. Highly stable exciton states at room temperature were discovered, whose binding energies are greater than 1 eV. The SBH at the WS_2−Au/Cr junction can be reduced by increasing the thickness of the WS_2, from 0.37 eV for the monolayer to 0.17 eV for the 28-layer WS_2. Precisely extracted values for n and k also exhibit unusual variation with the thickness. This discovery suggests that the optical and electronic properties of WS_2, or generally TMDs, can be modulated by changing the number of layers of WS_2. Engineering the material properties according to the number of layers can be a novel pathway uniquely adaptable to TMDs.

MATERIALS AND METHODS

Transfer of Few-Layer WS_2 to Other Substrates. The WS_2 flakes were transferred using the mechanical-exfoliation method. After locating the few-layer WS_2 flakes, AFM (park systems) is used to measure the thickness in noncontact mode under ambient conditions. Then, the flakes were transferred to other substrates with different thicknesses of SiO_2 (2.9−302 nm) by the following steps.[41] Optical images were obtained using a Nikon eclipse LV150 with an optional optical filter. The intensity of the image was obtained using ImageJ software.

Raman and Photoluminescence (PL) Measurement. For Raman and PL measurements, the 514.4 nm (2.41 eV) line of a diode-pumped-solid-state laser was used as an excitation source. The laser beam was focused onto the sample by a 50× microscope objective lens (0.8 Numerical Aperture), and the scattered light was collected and collimated by the same lens. The scattered signal was dispersed using a Jobin-Yvon Triax 320 spectrometer (1200 grooves/mm for Raman,

300 grooves/mm for PL measurements) and detected by a thermoelectrically cooled, back-illuminated, deep-depletion charge-coupled device detector. The laser power was maintained below 0.2 mW to avoid the local heating effect.

Device Fabrication and Electrical Measurement. E-beam lithography was used to define the patterns of the electrodes followed by the development of the patterns using a mixture of MIBK and IPA (MIBK 1:IPA 3). Using an e-beam evaporator, 20 nm Cr and then 50 nm Au were deposited in a high vacuum ($\sim10^{-6}$ Torr). The current–voltage characteristic of the devices was measured using a Keithley 4200 semiconductor parameter analyzer in a high vacuum ($\sim10^{-6}$ Torr). The temperature was changed from 260 to 380 K using liquid nitrogen. Light was blocked to minimize the photocurrent effect due to the metal–WS_2 junction. The IL was a mixture of 1-ethyl-3-methylimidazolium bis(trifluoromethylsulfonyl)imide: [EMIM][TFSI] ionic liquid, poly(ethylene glycol) diacrylate(PEG-DA) monomer, and 2-hydroxy-2-methylpropiophenone (HOMPP) at a ratio of 88:8:4 (w/w).[42]

Conflict of Interest: The authors declare no competing financial interest.

Supporting Information Available: Additional information about the precise measurement of the SiO_2 thickness, bandgap estimation using the refractive index, and bandgap extraction using the ionic liquid-gating method. The Supporting Information is available free of charge on the ACS Publications website at DOI: 10.1021/acsnano.5b01727.

Acknowledgment. The authors thank Y.-W. Son for insightful discussions. This research was supported by the Basic Science Research Program through the National Research Foundation of Korea (NRF), funded by MSIP (NRF-2013R1A1A1058581, 2011-0013461 and 2011-0017605), the Center for Advanced Soft-Electronics, funded by MSIP as Global Frontier Project (CASE-2011-0031640 and 2011-0031630), and the BSR2012R1A2A2A01045496, which is supported by the NRF and funded by the Ministry of Education, Science and Technology. Bae Ho Park was supported by NRF of Korea grants funded by the Korea government (MSIP) (No. 2013R1A3A2042120).

REFERENCES AND NOTES

1. Georgiou, T.; Jalil, R.; Belle, B. D.; Britnell, L.; Gorbachev, R. V.; Morozov, S. V.; Kim, Y. J.; Gholinia, A.; Haigh, S. J.; Makarovsky, O.; Eaves, L.; Ponomarenko, L. A.; Geim, A. K.; Novoselov, K. S.; Mishchenko, A. Vertical field-effect transistor based on graphene-WS_2 heterostructures for flexible and transparent electronics. *Nat. Nanotechnol.* **2013**, *8*, 100–103.
2. Yu, W. J.; Li, Z.; Zhou, H.; Chen, Y.; Wang, Y.; Huang, Y.; Duan, X. Vertically stacked multi-heterostructures of layered materials for logic transistors and complementary inverters. *Nat. Mater.* **2013**, *12*, 246–252.
3. Wang, Q. H.; Kalantar-Zadeh, K.; Kis, A.; Coleman, J. N.; Strano, M. S. Electronics and optoelectronics of two-dimensional transition metal dichalcogenides. *Nat. Nanotechnol.* **2012**, *7*, 699–712.
4. Yang, H.; Heo, J.; Park, S.; Song, H. J.; Seo, D. H.; Byun, K. E.; Kim, P.; Yoo, I.; Chung, H. J.; Kim, K. Graphene barristor, a triode device with a gate-controlled Schottky barrier. *Science* **2012**, *336*, 1140–1143.
5. Tian, H.; Tan, Z.; Wu, C.; Wang, X.; Mohammad, M. A.; Xie, D.; Yang, Y.; Wang, J.; Li, L. J.; Xu, J.; Ren, T. L. Novel Field-Effect Schottky Barrier Transistors Based on Graphene-MoS_2 Heterojunctions. *Sci. Rep.* **2014**, *4*, 5951.
6. Shanmugam, M.; Bansal, T.; Durcan, C. A.; Yu, B. Schottky-barrier solar cell based on layered semiconductor tungsten disulfide nanofilm. *Appl. Phys. Lett.* **2012**, *101*, 263902.
7. Yu, W. J.; Liu, Y.; Zhou, H.; Yin, A.; Li, Z.; Huang, Y.; Duan, X. Highly efficient gate-tunable photocurrent generation in vertical heterostructures of layered materials. *Nat. Nanotechnol.* **2013**, *8*, 952–958.
8. Kang, J.; Tongay, S.; Zhou, J.; Li, J.; Wu, J. Band offsets and heterostructures of two-dimensional semiconductors. *Appl. Phys. Lett.* **2013**, *102*, 012111.
9. Kuc, A.; Zibouche, N.; Heine, T. Influence of quantum confinement on the electronic structure of the transition metal sulfide TS_2. *Phys. Rev. B: Condens. Matter Mater. Phys.* **2011**, *83*, 245213.
10. Shi, H.; Pan, H.; Zhang, Y.-W.; Yakobson, B. Quasiparticle band structures and optical properties of strained monolayer MoS_2 and WS_2. *Phys. Rev. B: Condens. Matter Mater. Phys.* **2013**, *87*, 155304.
11. Xi, Q.; Zhou, D.-M.; Kan, Y.-Y.; Ge, J.; Wu, Z.-K.; Yu, R.-Q.; Jiang, J.-H. Highly Sensitive and Selective Strategy for MicroRNA Detection Based on WS_2 Nanosheet Mediated Fluorescence Quenching and Duplex-Specific Nuclease Signal Amplification. *Anal. Chem.* **2014**, *86*, 1361–1365.
12. Lopez-Sanchez, O.; Lembke, D.; Kayci, M.; Radenovic, A.; Kis, A. Ultrasensitive photodetectors based on monolayer MoS_2. *Nat. Nanotechnol.* **2013**, *8*, 497–501.
13. Zhang, X.; Liang, J.; Ding, S. The Application of Nanostructure MoS_2 Materials in Energy Storage and Conversion. In *MoS_2*; Springer: Cham, Switzerland, 2014; Vol. 21, pp 237–268.
14. Wang, H.; Lu, Z.; Xu, S.; Kong, D.; Cha, J. J.; Zheng, G.; Hsu, P.-C.; Yan, K.; Bradshaw, D.; Prinz, F. B. Electrochemical tuning of vertically aligned MoS_2 nanofilms and its application in improving hydrogen evolution reaction. *Proc. Natl. Acad. Sci. U. S. A.* **2013**, *110*, 19701–19706.
15. Hong, X.; Kim, J.; Shi, S.-F.; Zhang, Y.; Jin, C.; Sun, Y.; Tongay, S.; Wu, J.; Zhang, Y.; Wang, F. Ultrafast charge transfer in atomically thin MoS_2/WS_2 heterostructures. *Nat. Nanotechnol.* **2014**, *9*, 682–686.
16. Jo, S.; Ubrig, N.; Berger, H.; Kuzmenko, A. B.; Morpurgo, A. F. Mono- and bilayer WS_2 light-emitting transistors. *Nano Lett.* **2014**, *14*, 2019–2025.
17. Hanbicki, A.; Currie, M.; Kioseoglou, G.; Friedman, A.; Jonker, B. Measurement of high exciton binding energy in the monolayer transition-metal dichalcogenides WS_2 and WSe_2. *Solid State Commun.* **2015**, *203*, 16–20.
18. Ramasubramaniam, A. Large excitonic effects in monolayers of molybdenum and tungsten dichalcogenides. *Phys. Rev. B: Condens. Matter Mater. Phys.* **2012**, *86*, 115409.
19. Ye, Z.; Cao, T.; O'Brien, K.; Zhu, H.; Yin, X.; Wang, Y.; Louie, S. G.; Zhang, X. Probing excitonic dark states in single-layer tungsten disulphide. *Nature* **2014**, *513*, 214–218.
20. Zhu, B.; Chen, X.; Cui, X. Exciton Binding Energy of Monolayer WS_2. *Sci. Rep.* **2015**, *5*, 9218.
21. Ugeda, M. M.; Bradley, A. J.; Shi, S.-F.; Felipe, H.; Zhang, Y.; Qiu, D. Y.; Ruan, W.; Mo, S.-K.; Hussain, Z.; Shen, Z.-X. Giant bandgap renormalization and excitonic effects in a monolayer transition metal dichalcogenide semiconductor. *Nat. Mater.* **2014**, *13*, 1091–1095.
22. Zhang, C.; Johnson, A.; Hsu, C.-L.; Li, L.-J.; Shih, C.-K. Direct imaging of band profile in single layer MoS2 on graphite: quasiparticle energy gap, metallic edge states, and edge band bending. *Nano Lett.* **2014**, *14*, 2443–2447.
23. Alfihed, S.; Hossain, M.; Alharbi, A.; Alyamani, A.; Alharbi, F. H. PLD Grown Polycrystalline Tungsten Disulphide (WS_2) Films. *J. Mater.* **2013**, *2013*, 1–5.
24. Byun, K.-E.; Chung, H.-J.; Lee, J.; Yang, H.; Song, H. J.; Heo, J.; Seo, D. H.; Park, S.; Hwang, S. W.; Yoo, I. Graphene for true ohmic contact at metal–semiconductor junctions. *Nano Lett.* **2013**, *13*, 4001–4005.
25. Blake, P.; Hill, E. W.; Castro Neto, A. H.; Novoselov, K. S.; Jiang, D.; Yang, R.; Booth, T. J.; Geim, A. K. Making graphene visible. *Appl. Phys. Lett.* **2007**, *91*, 063124.
26. Gorbachev, R. V.; Riaz, I.; Nair, R. R.; Jalil, R.; Britnell, L.; Belle, B. D.; Hill, E. W.; Novoselov, K. S.; Watanabe, K.; Taniguchi, T. Hunting for monolayer boron nitride: optical and Raman signatures. *Small* **2011**, *7*, 465–468.
27. Benameur, M. M.; Radisavljevic, B.; Heron, J. S.; Sahoo, S.; Berger, H.; Kis, A. Visibility of dichalcogenide nanolayers. *Nanotechnology* **2011**, *22*, 125706.
28. Ishigami, M.; Chen, J.; Cullen, W.; Fuhrer, M.; Williams, E. Atomic structure of graphene on SiO_2. *Nano Lett.* **2007**, *7*, 1643–1648.
29. Lee, C.; Yan, H.; Brus, L. E.; Heinz, T. F.; Hone, J.; Ryu, S. Anomalous Lattice Vibrations of Single- and Few-Layer MoS_2. *ACS Nano* **2010**, *4*, 2695–2700.

30. Berkdemir, A.; Gutiérrez, H. R.; Botello-Méndez, A. R.; Perea-López, N.; Elías, A. L.; Chia, C.-I.; Wang, B.; Crespi, V. H.; López-Urías, F.; Charlier, J.-C.; Terrones, H.; Terrones, M. Identification of individual and few layers of WS_2 using Raman Spectroscopy. *Sci. Rep.* **2013**, *3*, 1755.
31. Nguyen, T. A.; Lee, J.-U.; Yoon, D.; Cheong, H. Excitation Energy Dependent Raman Signatures of ABA- and ABC-stacked Few-layer Graphene. *Sci. Rep.* **2014**, *4*, 4630.
32. Zhao, W.; Ghorannevis, Z.; Amara, K. K.; Pang, J. R.; Toh, M.; Zhang, X.; Kloc, C.; Tan, P. H.; Eda, G. Lattice dynamics in mono- and few-layer sheets of WS_2 and WSe_2. *Nanoscale* **2013**, *5*, 9677–9683.
33. Maeda, Y.; Tsukamoto, N.; Yazawa, Y.; Kanemitsu, Y.; Masumoto, Y. Visible photoluminescence of Ge microcrystals embedded in SiO_2 glassy matrices. *Appl. Phys. Lett.* **1991**, *59*, 3168–3170.
34. Qiu, D. Y.; da Jornada, F. H.; Louie, S. G. Optical Spectrum of MoS_2: Many-Body Effects and Diversity of Exciton States. *Phys. Rev. Lett.* **2013**, *111*, 216805.
35. Berkelbach, T. C.; Hybertsen, M. S.; Reichman, D. R. Theory of neutral and charged excitons in monolayer transition metal dichalcogenides. *Phys. Rev. B: Condens. Matter Mater. Phys.* **2013**, *88*, 045318.
36. Zhao, W.; Ghorannevis, Z.; Chu, L.; Toh, M.; Kloc, C.; Tan, P.-H.; Eda, G. Evolution of electronic structure in atomically thin sheets of WS_2 and WSe_2. *ACS Nano* **2013**, *7*, 791–797.
37. Zhao, W.; Ribeiro, R. M.; Toh, M.; Carvalho, A.; Kloc, C.; Castro Neto, A. H.; Eda, G. Origin of Indirect Optical Transitions in Few-Layer MoS_2, WS_2, and WSe_2. *Nano Lett.* **2013**, *13*, 5627–5634.
38. Braga, D.; Gutierrez Lezama, I.; Berger, H.; Morpurgo, A. F. Quantitative determination of the band gap of WS_2 with ambipolar ionic liquid-gated transistors. *Nano Lett.* **2012**, *12*, 5218–5223.
39. Chernikov, A.; Berkelbach, T. C.; Hill, H. M.; Rigosi, A.; Li, Y.; Aslan, O. B.; Reichman, D. R.; Hybertsen, M. S.; Heinz, T. F. Exciton Binding Energy and Nonhydrogenic Rydberg Series in Monolayer WS_2. *Phys. Rev. Lett.* **2014**, *113*, 076802.
40. Schroder, D. K. *Semiconductor Material and Device Characterization*; John Wiley & Sons: New York, 2006.
41. Kim, H.; Yun, H.; Yoon, H. A.; Lee, S. W. Integrating ZnO Microwires with Nanoscale Electrodes Using a Suspended PMMA Ribbon for Studying Reliable Electrical and Electromechanical Properties. *Adv. Energy Mater.* **2014**, *4*, 1301973.
42. Lee, S. W.; Lee, H. J.; Choi, J. H.; Koh, W. G.; Myoung, J. M.; Hur, J. H.; Park, J. J.; Cho, J. H.; Jeong, U. Periodic array of polyelectrolyte-gated organic transistors from electrospun poly (3-hexylthiophene) nanofibers. *Nano Lett.* **2010**, *10*, 347–351.